ships. This protocol was repeated in Krebs solution with 6.5 mM K^+. To identify the postsynaptic leptin current, *I–V* relationships were performed similarly with slow voltage ramps (5 mV s^{-1} from −100 to −20 mV) before and 10 min after adding leptin (100 nM).

GABA-mediated IPSCs were recorded using a CsCl internal electrode solution ((in mM): 140 CsCl, 10 HEPES, 5 $MgCl_2$, 1 BAPTA, 5 Mg-ATP, 0.3 Na-GTP). Both mini IPSCs and large amplitude (presumably multisynaptic) IPSCs were observed in the untreated slices. TTX (1 μM) abolished large IPSCs. We acquired data before and after drug addition at a −50-mV holding potential in 2-s sweeps every 4 s for the times indicated in the figures. Mini-postsynaptic currents were analysed using Axograph 4 (Axon Instruments). IPSCs and excitatory postsynaptic currents (EPSCs) were distinguished on the basis of their decay constants; in addition, picrotoxin (100 μM) blocked all IPSCs. POMC neurons receive a low EPSC tone, and the frequency was not modulated by any of the treatments described here.

Immunostaining for light and electron microscopy

We carried out double immunocytochemistry for NPY and POMC using different colour diaminobenzidine (DAB) chromogens on fixed mouse hypothalami according to published protocols[27]. For electron microscopy, pre-embedding immunostaining for β-endorphin was done with an ABC Elite kit (Vector Laboratories) and a DAB reaction, followed by post-embedding labelling of GABA and NPY using rabbit anti-GABA, 1:1000 (v/v), and gold-conjugated (10-nm) goat anti-rabbit IgG or sheep anti-NPY and gold-conjugated (25-nm) goat anti-sheep IgG. Sections were contrasted with saturated uranyl acetate (10 min) and lead citrate (20–30 s), and examined using a Philips CM-10 electron microscope.

Received 19 December 2000; accepted 12 March 2001.

1. Zhang, Y. *et al.* Positional cloning of the mouse obese gene and its human homologue. *Nature* **372,** 425–432 (1994); erratum *ibid.* **374,** 479 (1995).
2. Farooqi, I. S. *et al.* Effects of recombinant leptin therapy in a child with congenital leptin deficiency. *N. Engl. J. Med.* **341,** 879–884 (1999).
3. Campfield, L. A., Smith, F. J., Guisez, Y., Devos, R. & Burn, P. Recombinant mouse OB protein: evidence for a peripheral signal linking adiposity and central neural networks. *Science* **269,** 546–549 (1995).
4. Kim, M. S. *et al.* The central melanocortin system affects the hypothalamo-pituitary thyroid axis and may mediate the effect of leptin. *J. Clin. Invest.* **105,** 1005–1011 (2000).
5. Haynes, W. G., Morgan, D. A., Walsh, S. A., Mark, A. L. & Sivitz, W. I. Receptor-mediated regional sympathetic nerve activation by leptin. *J. Clin. Invest.* **100,** 270–278 (1997).
6. Haynes, W. G., Morgan, D. A., Djalali, A., Sivitz, W. I. & Mark, A. L. Interactions between the melanocortin system and leptin in control of sympathetic nerve traffic. *Hypertension* **33,** 542–547 (1999).
7. Hakansson, M. L., Brown, H., Ghilardi, N., Skoda, R. C. & Meister, B. Leptin receptor immunoreactivity in chemically defined target neurons of the hypothalamus. *J. Neurosci.* **18,** 559–572 (1998).
8. Kalra, S. P. *et al.* Interacting appetite-regulating pathways in the hypothalamic regulation of body weight. *Endocr. Rev.* **20,** 68–100 (1999).
9. Cone, R. D. The central melanocortin system and energy homeostasis. *Trends Endocrinol. Metab.* **10,** 211–216 (1999).
10. Elias, C. F. *et al.* Leptin differentially regulates NPY and POMC neurons projecting to the lateral hypothalamic area. *Neuron* **23,** 775–786 (1999).
11. Glaum, S. R. *et al.* Leptin, the obese gene product, rapidly modulates synaptic transmission in the hypothalamus. *Mol. Pharmacol.* **50,** 230–235 (1996).
12. Spanswick, D., Smith, M. A., Groppi, V. E., Logan, S. D. & Ashford, M. L. Leptin inhibits hypothalamic neurons by activation of ATP-sensitive potassium channels. *Nature* **390,** 521–525 (1997).
13. Lee, K., Dixon, A. K., Richardson, P. J. & Pinnock, R. D. Glucose-receptive neurones in the rat ventromedial hypothalamus express KATP channels composed of Kir6.1 and SUR1 subunits. *J. Physiol. (Lond.)* **515,** 439–452 (1999).
14. Shiraishi, T., Sasaki, K., Niijima, A. & Oomura, Y. Leptin effects on feeding-related hypothalamic and peripheral neuronal activities in normal and obese rats. *Nutrition* **15,** 576–579 (1999).
15. Bagnol, D. *et al.* Anatomy of an endogenous antagonist: relationship between Agouti-related protein and proopiomelanocortin in brain. *J. Neurosci.* [online] (cited 25 Aug. 99) <http://www.jneurosci.org/cgi/content/full/19/18/RC26> (1999).
16. Butler, A. A. *et al.* A unique metabolic syndrome causes obesity in the melanocortin-3 receptor-deficient mouse. *Endocrinology* **141,** 3518–3521 (2000).
17. Young, J. I. *et al.* Authentic cell-specific and developmentally regulated expression of pro-opiomelanocortin genomic fragments in hypothalamic and hindbrain neurons of transgenic mice. *J. Neurosci.* **18,** 6631–6640 (1998).
18. Franklin, K. B. J. & Paxinos, G. *The Mouse Brain in Stereotaxic Coordinates* (Academic, San Diego, 1997).
19. Kelly, M. J., Loose, M. D. & Ronnekleiv, O. K. Opioids hyperpolarize β-endorphin neurons via μ-receptor activation of a potassium conductance. *Neuroendocrinology* **52,** 268–275 (1990).
20. Slugg, R. M., Hayward, M. D., Ronnekleiv, O. K., Low, M. J. & Kelly, M. J. Effect of the μ-opioid agonist DAMGO on medial basal hypothalamic neurons in β-endorphin knock-out mice. *Neuroendocrinology* **72,** 208–217 (2000).
21. Powis, J. E., Bains, J. S. & Ferguson, A. V. Leptin depolarizes rat hypothalamic paraventricular nucleus neurons. *Am. J. Physiol.* **274,** R1468–R1472 (1998).
22. Horvath, T. L., Bechmann, I., Naftolin, F., Kalra, S. P. & Leranth, C. Heterogeneity in the neuropeptide Y-containing neurons of the rat arcuate nucleus: GABAergic and non-GABAergic subpopulations. *Brain Res.* **756,** 283–286 (1997).
23. Broberger, C., Landry, M., Wong, H., Walsh, J. N. & Hokfelt, T. Subtypes Y1 and Y2 of the neuropeptide Y receptor are respectively expressed in pro-opiomelanocortin- and neuropeptide-Y-containing neurons of the rat hypothalamic arcuate nucleus. *Neuroendocrinology* **66,** 393–408 (1997).
24. King, P. J., Widdowson, P. S., Doods, H. N. & Williams, G. Regulation of neuropeptide Y release by neuropeptide Y receptor ligands and calcium channel antagonists in hypothalamic slices. *J. Neurochem.* **73,** 641–646 (1999).
25. Grieco, P., Balse, P. M., Weinberg, D., MacNeil, T. & Hruby, V. J. D-Amino acid scan of gamma-melanocyte-stimulating hormone: importance of Trp(8) on human MC3 receptor selectivity. *J. Med. Chem.* **43,** 4998–5002 (2000).
26. Csiffary, A., Gorcs, T. J. & Palkovits, M. Neuropeptide Y innervation of ACTH-immunoreactive neurons in the arcuate nucleus of rats: a correlated light and electron microscopic double immunolabeling study. *Brain Res.* **506,** 215–222 (1990).
27. Horvath, T. L., Naftolin, F. & Leranth, C. GABAergic and catecholaminergic innervation of mediobasal hypothalamic beta-endorphin cells projecting to the medial preoptic area. *Neuroscience* **51,** 391–399 (1992).
28. Cowley, M. A. *et al.* Integration of NPY, AGRP, and melanocortin signals in the hypothalamic paraventricular nucleus: evidence of a cellular basis for the adipostat. *Neuron* **24,** 155–163 (1999).
29. Halaas, J. L. *et al.* Physiological response to long-term peripheral and central leptin infusion in lean and obese mice. *Proc. Natl Acad. Sci. USA* **94,** 8878–8883 (1997).

Acknowledgements

We wish to thank V. J. Hruby for the D-Trp^8-γMSH, O. K. Ronnekliev, R. G. Allen and M. R. Brown for antisera and J. T. Williams and J. M. Brundege for advice. This work was supported by the NIH, a Fogarty International Research Collaborative Award, the International Scholar Program of the Howard Hughes Medical Institute, and Agencia Nacional de Promoción Cientifica y Technológica.

Correspondence and requests for materials should be addressed to R.D.C. (e-mail: cone@ohsu.edu) or M.J.L. (e-mail: low@ohsu.edu).

Calmodulin bifurcates the local Ca^{2+} signal that modulates P/Q-type Ca^{2+} channels

Carla D. DeMaria*, Tuck Wah Soong†, Badr A. Alseikhan*, Rebecca S. Alvania* & David T. Yue*

* *The Johns Hopkins University School of Medicine, Departments of Biomedical Engineering and Neuroscience, Program in Molecular and Cellular Systems Physiology, 720 Rutland Avenue, Baltimore, Maryland 21205, USA*
† *National Neuroscience Institute, 11 Jalan Tan Tuck Seng, Singapore 308433, and Department of Physiology, National University of Singapore*

Acute modulation of P/Q-type (α_{1A}) calcium channels by neuronal activity-dependent changes in intracellular Ca^{2+} concentration may contribute to short-term synaptic plasticity[1–3], potentially enriching the neurocomputational capabilities of the brain[4,5]. An unconventional mechanism for such channel modulation has been proposed[6,7] in which calmodulin (CaM) may exert two opposing effects on individual channels, initially promoting ('facilitation') and then inhibiting ('inactivation') channel opening. Here we report that such dual regulation arises from surprising Ca^{2+}-transduction capabilities of CaM. First, although facilitation and inactivation are two competing processes, both require Ca^{2+}-CaM binding to a single 'IQ-like' domain on the carboxy tail of α_{1A}[8]; a previously identified 'CBD' CaM-binding site[6,7] has no detectable role. Second, expression of a CaM mutant with impairment of all four of its Ca^{2+}-binding sites (CaM_{1234}) eliminates both forms of modulation. This result confirms that CaM is the Ca^{2+} sensor for channel regulation, and indicates that CaM may associate with the channel even before local Ca^{2+} concentration rises. Finally, the bifunctional capability of CaM arises from bifurcation of Ca^{2+} signalling by the lobes of CaM: Ca^{2+} binding to the amino-terminal lobe selectively initiates channel inactivation, whereas Ca^{2+} sensing by the carboxy-terminal lobe induces facilitation. Such lobe-specific detection provides a compact means to decode local Ca^{2+} signals in two ways, and to separately initiate distinct actions on a single molecular complex.

To simplify the dissection of the molecular mechanisms, we studied recombinant P/Q-type ($\alpha_{1A}/\beta_{2a}/\alpha_2\delta$) channels expressed in mammalian HEK293 cells. Figure 1a shows that Ca^{2+}-dependent

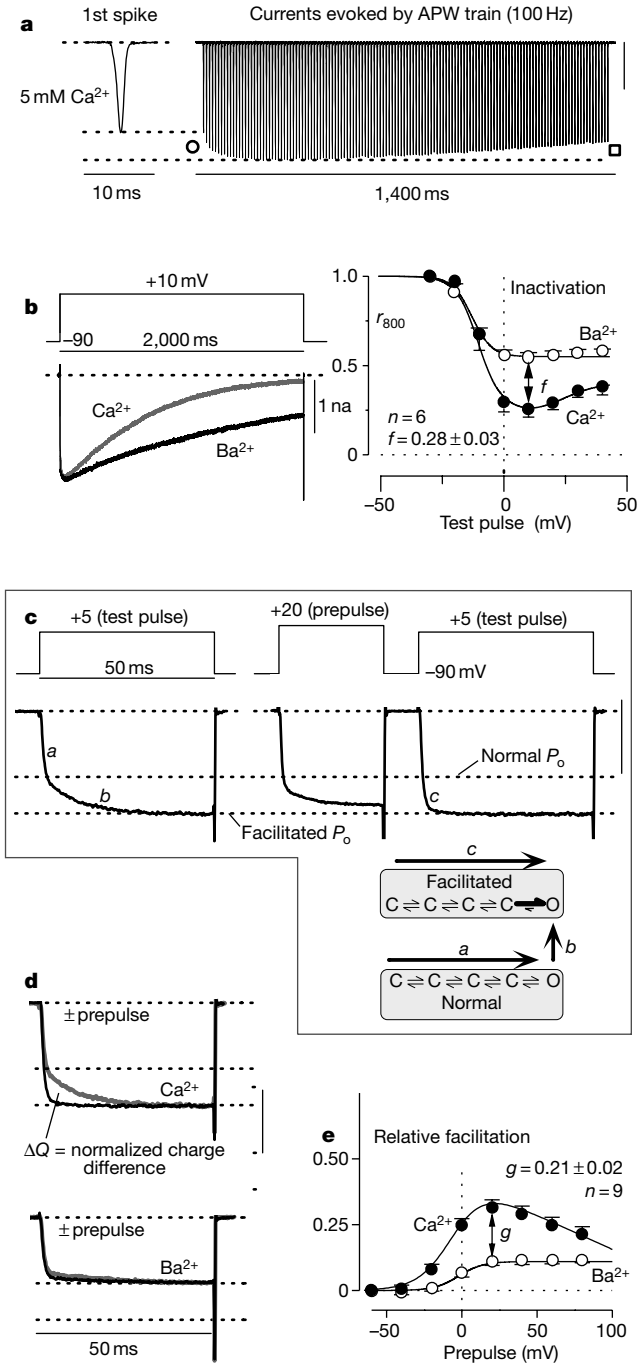

Figure 1 Facilitation and inactivation in P/Q-type Ca^{2+} channels. **a**, Ca^{2+} currents show facilitation (circle) and inactivation (square) during trains of action potential waveforms (APW). **b**, Left, inactivation of Ca^{2+} (grey) and Ba^{2+} (black) currents during step depolarization. Ca^{2+} traces for inactivation amplified about twice to match Ba^{2+} traces, and tail currents clipped at borders. Ba^{2+} scale, 1 nA. Right, r_{800}, averaged from n cells. f was taken at 10 mV. **c**, Ca^{2+}-dependent facilitation in prepulse protocols. Left, test pulse without prepulse. Right, test pulse following prepulse, with rapid activation to larger facilitated level. Ca^{2+} scale, 1 nA. P_0, steady-state open probability. Same cell as in **b** was used. Bottom, interpretation of phases *a*–*c*. *a*, Initial rapid activation; *b*, slower phase of increase; *c*, the channels already in the facilitated mode rapidly activate. **d**, Quantification of facilitation. Top, test-pulse Ca^{2+} currents obtained without (grey) and with (black) prepulse, from **c** after normalization to unity at test-pulse termination. ΔQ, integral of difference between normalized traces. Relative facilitation RF = $\Delta Q/\tau = 0.33$ for upper traces, where τ is the facilitation time constant (~10 ms) (see Methods). Bottom, test-pulse Ba^{2+} currents, same cell (RF = 0.11). Scale, 2 nA. Ba^{2+} traces scaled to reflect lower open probability of normal mode. **e**, Average relative facilitation. g taken at 20 mV. **a**–**e**, See Supplementary Information.

facilitation and inactivation in such recombinant channels recapitulate modulatory behaviour compatible with that of presynaptic channels[1,2]. To mimic physiological responses, we activated recombinant channels using trains of action-potential waveforms. The resulting Ca^{2+} currents facilitated with repetitive spikes, and then inactivated over a longer timescale. Such behaviour was absent in corresponding Ba^{2+} currents (see Supplementary Information), fitting with the high selectivity of CaM[9] for Ca^{2+} over Ba^{2+}.

To quantify the inactivation, we used prolonged square-pulse depolarizations (Fig. 1b, left), in which Ca^{2+} current decayed almost completely whereas the corresponding Ba^{2+} current remained substantial. On average (Fig. 1b, right), the fraction of peak Ca^{2+} current present after depolarizing for 800 ms (r_{800}) bore a deep, U-shaped dependence upon test-pulse voltage, consistent with genuine Ca^{2+}-dependent inactivation[8]. The corresponding Ba^{2+} relation declined only modestly, reflecting a slower voltage-dependent mechanism. Hence, the difference between Ca^{2+} and Ba^{2+} $r_{800}(f)$ provided a robust index of pure Ca^{2+}-dependent inactivation.

Using shorter pulses with negligible inactivation (Fig. 1c, left top), facilitation was readily resolved as a slower phase of Ca^{2+} current increase (*b*), following an initial rapid activation (*a*). The phenomenon could be understood as fast activation in a normal mode of gating (Fig. 1c, bottom, pathway *a*), followed by slower, Ca^{2+}-driven conversion to a facilitated gating mode with enhanced open probability (pathway *b*). Such a scenario was confirmed in three ways. First, a voltage prepulse should 'prefacilitate' the

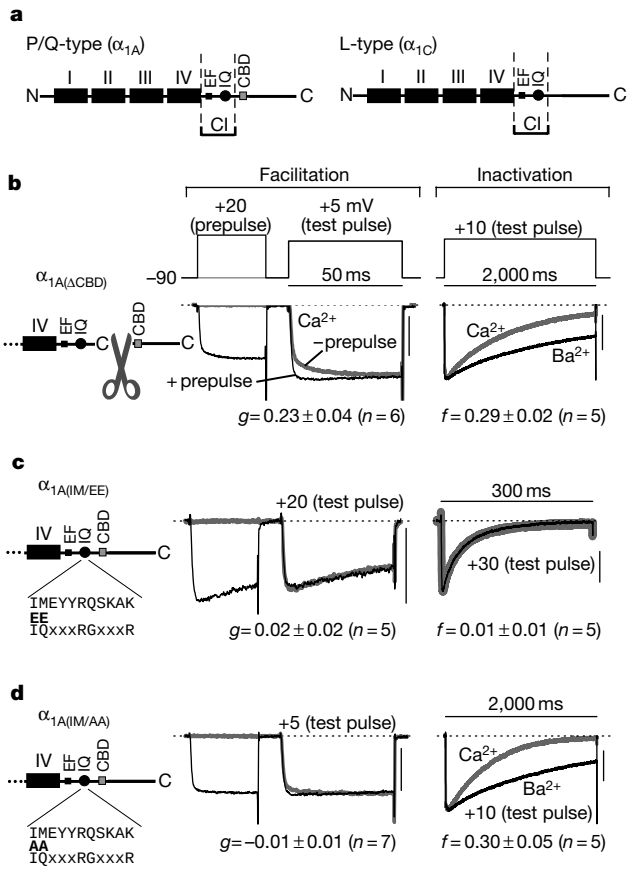

Figure 2 Structural determinants of facilitation and inactivation. **a**, P/Q-type and L-type channel pore-forming α_1-subunits. Channel domains (I–IV). Proximal third of C-tail (CI region) contains consensus EF-hand (EF), IQ motif (IQ) and CBD domain. **b**–**d**, Format essentially as in Fig. 1, except **c**. Scales, 1 nA, except prepulse in **c** (0.5 nA). **c**, IQ consensus[8] shown for reference. Higher charge carrier (Methods) necessitated different test-pulse voltages. Faster inactivation required shorter inactivation test pulses, and use of r_{100} (fraction of peak current after a 100-ms depolarization) to quantify inactivation. *f*, difference in Ba^{2+} and Ca^{2+} r_{100} at 30 mV. **a**–**d**, See Supplementary Information.

channels, such that a subsequent test pulse would rapidly activate the channels already in the facilitated gating mode (Fig. 1c, right and bottom, pathway *c*). The overlay of normalized test-pulse Ca^{2+} currents (obtained ± prepulse) underscores such prefacilitation (Fig. 1d, top). Second, test-pulse Ba^{2+} currents should activate by a single, rapid component regardless of prepulse depolarization (Fig. 1d, bottom), because of channel 'trapping' in the normal mode. Finally, if Ca^{2+} entry drives facilitation, then prefacilitation should bear a bell-shaped dependence upon prepulse potential (Fig. 1e). This was confirmed by the average relation between relative facilitation and prepulse voltage. Here, the relative facilitation is proportional to the fraction of channels facilitated by a prepulse, as relative facilitation is derived from the difference in charge (ΔQ; Fig. 1d) carried by normalized test-pulse currents (elicited ± prepulse; Fig. 1d). The corresponding Ba^{2+} relative facilitation (Fig. 1e) showed only a small monotonic increase, reflecting background G-protein modulation[10]. Hence, the difference between Ca^{2+} and Ba^{2+} relative facilitations (*g*; Fig. 1e) gave a measure of pure Ca^{2+}-dependent facilitation.

How does CaM initiate such kinetically disparate processes—facilitation and inactivation—on a single target molecule? One possibility is that Ca^{2+}-CaM binds to two channel sites, one for each modulatory effect. Although the CaM-binding domain (CBD) site on the distal carboxyl tail (C-tail) of α_{1A} reportedly mediated both facilitation and inactivation[6,7] (Fig. 2a, left), CaM also binds to an upstream IQ-like motif[8]. Though the function of the α_{1A} IQ site was unknown, CaM binding to the homologous L-type channel IQ site (Fig. 2a, right) is crucial to Ca^{2+} regulation[8,11–13], and the encompassing CI (calcium inactivation) region may transduce Ca^{2+}-CaM binding to L-type channel modulation[14].

To test for a functional role of sites outside the CBD, we truncated the α_{1A} C-tail so as to entirely remove the CBD region ($\alpha_{1A(\Delta CBD}$; Fig. 2b). Unexpectedly, facilitation and inactivation were not appreciably changed compared with the wild-type α_{1A}, implicating other CaM-binding sites in channel regulation. To test the importance of the α_{1A} IQ site, we mutated the critical isoleucine and methionine residues of the IQ-like motif[15] to negatively charged glutamates ($\alpha_{1A(IM/EE)}$; Fig. 2c), in an attempt to disrupt Ca^{2+}-CaM interaction. These mutations entirely abolished facilitation and inactivation, suggesting that both regulatory effects are initiated through Ca^{2+}-CaM interaction with the IQ site. The residual voltage-dependent inactivation, identical with either Ca^{2+} or Ba^{2+}, was accelerated about 40-fold. This fit with the dual roles of transduction and CaM binding served by many CaM-interaction domains[16] (see Supplementary Information). We also examined more modest mutations to neutrally charged alanines ($\alpha_{1A(IM/AA)}$; Fig. 2d), in an attempt to preserve partial Ca^{2+}-CaM interaction. Such mutations eliminated facilitation, but spared Ca^{2+}-dependent inactivation.

The presumed effects of channel mutations on Ca^{2+}-CaM interaction were verified by gel-mobility shift assays, in which mixtures of CaM and peptides spanning the α_{1A} IQ region were electrophoresed on nondenaturing gels (Fig. 3a–c). Without Ca^{2+}, CaM ran as a single, peptide-free band, regardless of the concentration of the wild-type peptide IQ_{WT} (Fig. 3a, left). By contrast, with Ca^{2+}, increasing peptide concentrations induced a graded interchange towards a slower mobility band (Fig. 3a, right), representing a peptide–Ca^{2+}-CaM complex. As we observed previously[8], the mobility shift saturated at low peptide:CaM ratios, indicating a substantial Ca^{2+}-CaM affinity for the peptide. By contrast, the $IQ_{IM/EE}$ peptide (Fig. 3b) showed no indication of peptide–CaM interaction, whereas the $IQ_{IM/AA}$ peptide (Fig. 3c) showed a partial mobility shift, indicating a modest interaction with Ca^{2+}-CaM. Fluorescence experiments with dansyl-CaM[17] (Fig. 3d) quantitatively confirmed this rank order of peptide–Ca^{2+}-CaM interaction. In saturating Ca^{2+}, IQ_{WT} bound CaM with high affinity ($K_d = 66$ nM), $IQ_{IM/AA}$ bound with intermediate affinity ($K_d = 1.03\ \mu M$) and $IQ_{IM/EE}$ showed no appreciable interaction. These biochemical studies (Fig. 3) confirmed the presumptions of functional mutational analysis in Fig. 2 (that IM/EE would eliminate, and IM/AA would weaken Ca^{2+}-CaM interaction), leading us to argue that Ca^{2+}-CaM binding to the α_{1A} IQ site alone mediates both facilitation and inactivation. The initial question about how the interaction of CaM with a single CBD site produces two modulatory effects was then replaced by a similar puzzle involving the IQ site.

The approach for solving this paradox came by first considering the fast kinetics of facilitation ($\tau \approx 10$ ms, Fig. 1c). Such rapidity seems incompatible with the diffuse cytoplasmic localization typical of CaM. Might apoCaM (Ca^{2+}-free CaM) be bound to the channel complex even before Ca^{2+} entry ('preassociation'), thus accelerating

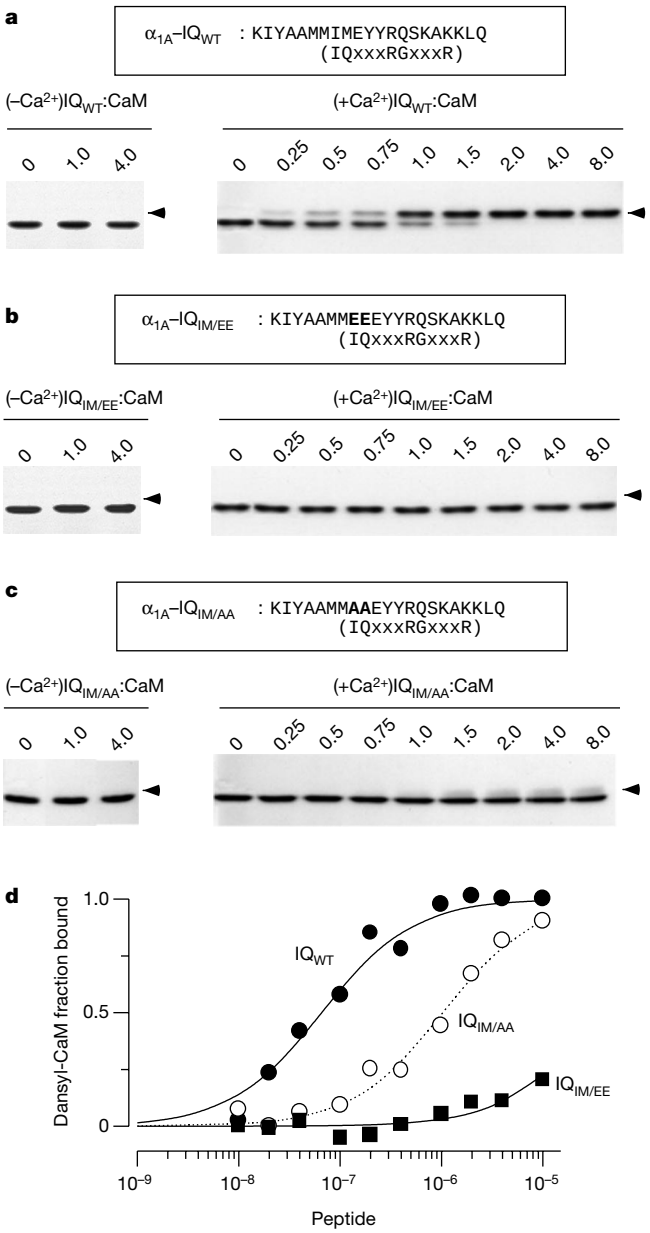

Figure 3 CaM binding to α_{1A} IQ site. **a**–**c**, Gel-mobility shift assay of CaM binding to peptides (insets) spanning the α_{1A} IQ site. Without Ca^{2+} (**a**–**c**, left), lack of CaM mobility shift. With Ca^{2+} (**a**–**c**, right), increasing IQ_{WT}:CaM ratios (**a**) caused exchange towards slower-mobility (peptide-Ca^{2+}-CaM) band (triangle); $IQ_{IM/EE}$ induced no shift in Ca^{2+} (**b**), and $IQ_{IM/AA}$ produced partial shift in Ca^{2+} (**c**). **d**, Dansyl-CaM fluorescence characterization of Ca^{2+}-CaM binding to peptides (see Methods). Smooth curves, single-binding isotherm fits.

subsequent Ca^{2+}-CaM interaction with the IQ site? To examine this question we coexpressed P/Q-type channels with CaM_{1234} (Fig. 4a, top), a Ca^{2+}-insensitive CaM mutant with aspartate-to-alanine mutations at the 'x' position of all four EF hands[8,18]. CaM_{1234} would eliminate channel regulation if the CaM responsible for modulation was prebound to the α_{1A} complex with preferential access to the IQ site; otherwise, functional endogenous CaM should preserve normal channel regulation[8]. The observed elimination of facilitation and inactivation (Fig. 4a) indicates preassociation of apoCaM, and unequivocally confirms that CaM is the Ca^{2+} sensor for regulation.

The dominant-negative action of CaM_{1234} allowed us to return to the question of how Ca^{2+}-CaM binding to a single IQ site initiates dual modulatory processes. Mutant CaMs with selective impairment of Ca^{2+} binding to either the N-terminal (CaM_{12}) or C-terminal lobe (CaM_{34}) (Fig. 4b, c, left) provided the key insight. Expression of CaM_{12}, in which the aspartate-to-alanine mutations described for CaM_{1234} were restricted to the N-terminal lobe, strikingly suppressed Ca^{2+}-dependent inactivation (Fig. 4b), whereas facilitation was indistinguishable from the control (Fig. 1e). Expression of CaM_{34} (Fig. 4c), in which the analogous mutations were restricted to the C-terminal lobe, yielded the opposite results: Ca^{2+}-dependent facilitation was essentially absent, whereas inactivation remained unchanged compared with the control (Fig. 1b). These unexpected findings were confirmed by additional population data (Fig. 4d) that gave the indices for the strength of inactivation (f) and facilitation (g); these were pooled from even more cells than were used for the full voltage protocols. We therefore conclude that Ca^{2+} binding to the N-terminal lobe of CaM selectively initiates inactivation, whereas Ca^{2+} binding to the C-terminal lobe selectively triggers facilitation.

Our experiments highlight signalling capabilities of CaM that may generalize to numerous biological systems. First, CaM regulation through the IQ-like site of α_{1A} adds to an emerging theme, as a homologous IQ site in L-type (α_{1C}) Ca^{2+} channels underlies their regulation by CaM[8,11–14], and analogous IQ-like motifs in R-type (α_{1E}) Ca^{2+} channels[8] and Na channels[19] interact with CaM. Second, preassociation of apoCaM with molecular complexes may be a prevalent mechanism to speed their modulation by Ca^{2+}-CaM. Both L-type Ca^{2+} channels[8,11] and small-conductance K channels[20,21] may exploit such a scheme. Moreover, FRET (fluorescence resonance energy transfer) experiments in our laboratory indicate a

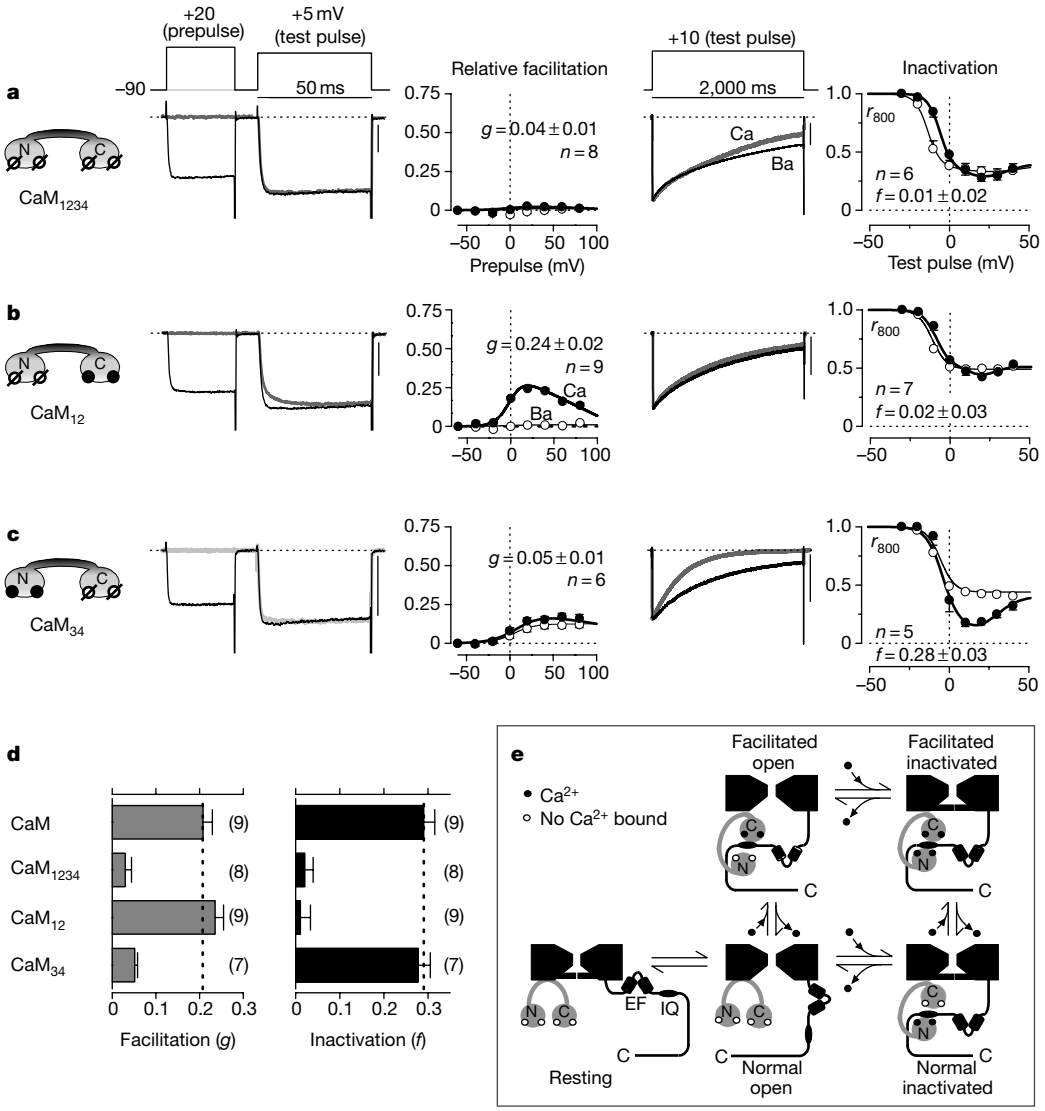

Figure 4 Selective initiation of facilitation and inactivation by different lobes of CaM. **a**–**c**, Format as in Fig. 1. Prepulse and Ba^{2+} inactivation scale, 1 nA. **a**, Co-expression of CaM_{1234} with channels. **b**, Co-expression of CaM_{12} (defective N-terminal lobe) with channels. **c**, Co-expression of CaM_{34} (defective C-terminal lobe) with channels. **d**, Summarized effects of various CaMs. CaM indicates endogenous CaM without recombinant expression. For each CaM, the same set of cells was used for facilitation and inactivation. **e**, Proposed mechanism of P/Q-type channel regulation. **a**–**e**, See Supplementary Information.

preassociation of CaM to multiple types of Ca^{2+} channels in living cells[22], and apoCaM binding sites have been identified in Na channels[19] and ryanodine receptors[23]. Third, our results show that CaM, acting through a single binding region, can use lobe-specific Ca^{2+} binding to selectively control distinct processes, perhaps as proposed for P/Q-type channels (Fig. 4e). ApoCaM preassociates with resting channels at a saturable site that provides preferential access to the IQ region. Depolarization opens channels, and the ensuing Ca^{2+} binding to the C-terminal lobe of CaM enables one form of interaction with the IQ site, which induces facilitated channel conformations. Ca^{2+} binding to the N-terminal lobe enables a second form of interaction that favours inactivated conformations. Selective elimination of inactivation or facilitation by CaM_{12} and CaM_{34} (Fig. 4d) shows that the processes are distinct. Such a mechanism could provide intriguing design advantages, especially because it seems likely that the lobes of CaM selectively detect features of the local Ca^{2+} signal that arise from local and distant sources of Ca^{2+} (Fig. 5). The C-terminal lobe may respond preferentially to the spike-like component of local Ca^{2+} concentration that is attributable to local channel activity (C-lobe CaM readout). The N-terminal lobe may detect the slow component of the signals which result from aggregate cellular Ca^{2+} signalling (N-lobe CaM readout) (see Supplementary Information). There are suggestive biochemical precedents for lobe-specific CaM signalling[16,24], and functional precedents where one lobe of CaM preferentially regulates *Paramecium*[25] and mammalian[8,20] channels, as well as yeast physiology[26]. However, the P/Q-type channel may provide the first example of CaM lobe-specific initiation of two regulatory effects on a single molecular target complex. If widespread, such bifurcation of local Ca^{2+} signals by CaM may be a critical rationale for the two-lobed design of calmodulin. □

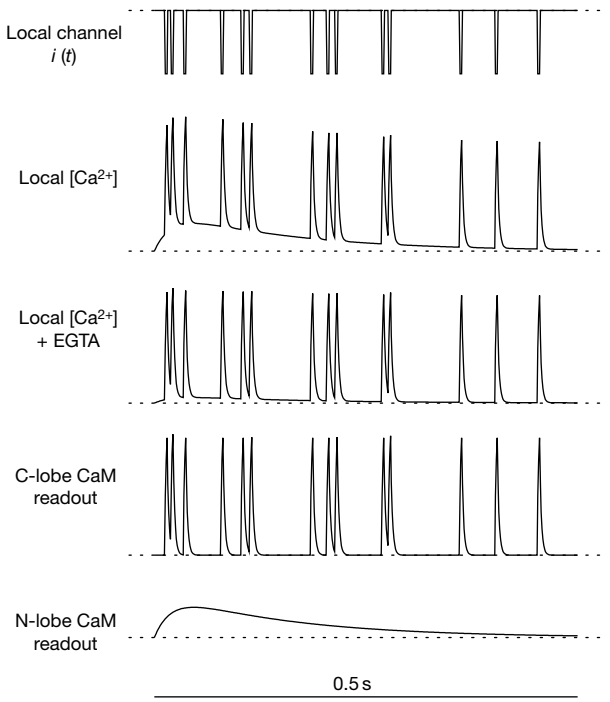

Figure 5 Decoding local Ca^{2+} concentrations ([Ca^{2+}]). Dotted lines, zero. Local channel $i(t)$, schematized currents of one Ca^{2+} channel. Theoretical local [Ca^{2+}] near channel[30], reflecting activity of associated channel (spikes) and distant Ca^{2+} sources (slow phase). Local [Ca^{2+}] + EGTA, postulated local Ca^{2+} with several mM cytoplasmic EGTA, featuring attenuation of slow phase with sparing of spikes[30]. C-lobe CaM readout, spike component. Deduction from sparing of facilitation with mM EGTA[7], facilitation dependence on CaM C-terminal lobe, and third trace. N-lobe CaM readout, slow phase. Deduction from inactivation blunting by mM EGTA[7], inactivation dependence on CaM N-terminal lobe, and third trace. Approximate timebase. See Supplementary Information.

Methods

Molecular biology

Mutations of the α_{1A} IQ-like region[8] (Fig. 2a, **I**MEYYRQSKAK) were made by PCR, with human α_{1A} as template[27]. For $\alpha_{1A(IM/EE)}$ and $\alpha_{1A(IM/AA)}$ mutants (Fig. 2c, d), forward mutagenic oligonucleotides spanned both the IQ region and a *Bgl*II site, 20 bp upstream of the reference isoleucine (bold). The reverse oligo had an *Xba*I site and sequence complementary to the α_{1A} stop codon. The resulting 899-base-pair (bp) PCR products were subcloned into human α_{1A}/pcDNA3 (Invitrogen) by *Bgl*II–*Xba*I. For $\alpha_{1A(\Delta CBD)}$ (Fig. 2b), the forward oligo annealed 44 bp upstream of an *Xho*I site preceding IVS6. The reverse oligo was complementary to the amino-acid stretch LDP, 51 amino acids downstream from the reference isoleucine. This was followed by a premature stop codon and *Xba*I site. The resulting 779-bp PCR fragment was subcloned into human α_{1A}/pcDNA3 by *Xho*I–*Xba*I. All PCR products were entirely sequenced. CaMs were cloned into pcDNA3 (ref. 8).

Gel-mobility-shift assay

CaM gel-shift assays were performed with 15% non-denaturing polyacrylamide gels mostly as described[8]. In Ca^{2+}-free experiments, 5 mM EGTA was added to reaction buffers and 2 mM EGTA was included in the running buffer, but no chelator or exogenous Ca^{2+} was added during gel casting. In experiments with Ca^{2+}, 1–2 mM Ca^{2+} was present in the reaction buffer and 0.1 mM Ca^{2+} was included in both the running buffer and gel (during casting).

Dansyl-CaM studies

Purified recombinant CaM protein was derivatized[28] with dansyl (5-dimethylamino-naphthalene-1-sulphonyl) chloride (Molecular Probes). The dansyl-CaM was then dialysed against 20 mM MOPS (pH 7.2). During binding assays, 100 nM dansyl-CaM was mixed with various concentrations of α_{1A}-IQ_{WT} peptide (Fig. 3a), in a room-temperature buffer[17] containing 2 mM $CaCl_2$, 150 mM NaCl and 50 mM Tris-Cl (pH 7.5). Comparable results were obtained with 150 μM $CaCl_2$ (not shown). Fluorescence emission (400–650 nm, 20 nm bandwidth) was monitored by a spectrofluorometer (SPF-500C, SLM Instruments), using 340 nm excitation (2.5 nm bandwidth). Background-subtracted fluorescence emission at 490 nm (F_{490}) specified the apparent fraction of CaM bound to peptide (B_{app}), with the relation $B_{app} = (F_{490} - F_{490}[\text{no peptide}])/(F_{490}[10\ \mu\text{M peptide}] - F_{490}[\text{no peptide}])$. This algorithm exploits a peptide-dependent blue shift and enhancement of dansyl emission spectra[17]. The relations between B_{app} and [α_{1A}-IQ_{WT} peptide] were least-squares fit with the relation $B_{app} = B_{app,max}/(K_d + [\alpha_{1A}\text{-}IQ_{WT}\ \text{peptide}])$, and the actual fraction of CaM bound to peptide determined as $B = B_{app}/B_{app,max}$ (Fig. 3d). We applied an analogous process to the relation between B_{app} and [α_{1A}-IQ_{IMIAA} peptide]. For the α_{1A}-$IQ_{IM/EE}$ peptide, the equation for B_{app} used a 100-μM peptide measurement (instead of a 10-μM). The peptides were from HHMI Biopolymer Laboratory, Johns Hopkins University School of Medicine.

Electrophysiology

The methods here were mostly as described[8]. cDNA for wild-type (or mutant) human α_{1A} (ref. 27) was transiently cotransfected with β_{2a} and α_{2b} (ref. 8) (and various CaMs[8] as required) in HEK293 cells. Two to three days later, whole-cell recordings were obtained at room temperature. β_{2a} minimized voltage inactivation[29], enhancing resolution of Ca^{2+}-dependent regulation. Bath solution contained (in mM): TEA-$MeSO_3$, 140; HEPES (pH 7.3), 10; and $CaCl_2$ or $BaCl_2$, 5; at 300 mOsm, adjusted with glucose. Internal solution (in mM): Cs-$MeSO_3$, 135; $CsCl_2$, 5; EGTA, 0.5; $MgCl_2$, 1; Mg–ATP, 4; and HEPES (pH 7.3), 10; at 290 mOsm, adjusted with glucose. To enhance the resolution of $\alpha_{1A(IM/EE)}$ (Fig. 2c), bath solution contained 20 mM $BaCl_2$ or $CaCl_2$ and 119 mM TEA-$MeSO_3$. Larger surface-potential shift caused by 20 mM charge carrier required increased test-pulse voltages (Fig. 2c). The protocols were otherwise the same as for the experiments with 5 mM charge carrier. For action potential waveforms (APWs) (Fig. 1a), voltages were precorrected for a −11 mV junction potential[10], with seals made in Ba^{2+} bath solution; otherwise, reported voltages were uncorrected, and true voltage may be obtained by subtracting 11 mV from reported values. APWs scaled uniformly from those recorded in calyx of Held[29], here with a 2-ms half width and a voltage range from −80 to 34 mV. Currents were filtered at 2 kHz and sampled at 10 kHz, except in APW experiments (5 kHz lowpass, 25 kHz sampling). Series resistance was typically 1–2 MΩ after more than 70% compensation. Leaks and capacitive transients were subtracted by P/8 protocol. Test-pulse depolarizations were delivered every 60 s (facilitation protocol) or 100 s (inactivation protocol).

Ca^{2+}-dependent facilitation was determined using the normalized charge difference ΔQ, obtained by integrating the difference between normalized traces ± prepulse (Fig. 1d, top). The fraction of channels facilitated by prepulse ($F_{facilitated}$) is directly proportional to ΔQ divided by the time constant (τ) of facilitation, yielding relative facilitation ($RF = \Delta Q/\tau$). This follows by assuming that all channels are initially in normal mode at test-pulse onset, and that subsequent shifts to facilitated mode occur mono-exponentially with a time constant τ. Then , $RF = F_{facilitated} \times [P_{o,facilitated} - P_{o,normal}]/P_{facilitated}$, where $P_{o,facilitated}$ and $P_{o,normal}$ are steady-state open probabilities in facilitated and normal modes, respectively. τ was explicitly determined from Ca^{2+} traces in each cell before calculation of RF. Ba^{2+} RF calculated by using τ values determined from Ca^{2+} traces in the same cell. For knockouts of facilitation (Figs 2c, d, 4a, c), τ was set to 10 ms (at about the average for control facilitation, Fig. 1d) in RF calculations.

All average data were presented as mean ± s.e.m., after analysis by custom-written software in MATLAB (MathWorks). Smooth-curve fits to data were done by eye, except in Fig. 3d. In Fig. 4, an important feature was to include only cells in which both g and f indices for facilitation and inactivation were determined. This constraint excluded the

possibility that selection bias might have led to an apparent differential elimination of regulatory mechanisms. Such an artefact could have occurred if mutant CaMs variably inhibited facilitation, inactivation, or both—depending on the particular cell under observation. Appropriate changes (or lack thereof) in *f* and *g* values, as determined from the same cells, excluded such a scenario (Fig. 4; see Supplementary Information).

Received 14 December 2000; accepted 30 March 2001.

1. Borst, J. G. & Sakmann, B. Facilitation of presynaptic calcium currents in the rat brainstem. *J. Physiol. (Lond.)* **513,** 149–155 (1998).
2. Cuttle, M. F., Tsujimoto, T., Forsythe, I. D. & Takahashi, T. Facilitation of the presynaptic calcium current at an auditory synapse in rat brainstem. *J. Physiol. (Lond.)* **512,** 723–729 (1998).
3. Forsythe, I. D., Tsujimoto, T., Barnes-Davies, M., Cuttle, M. & Takahashi, T. Inactivation of presynaptic calcium current contributes to synaptic depression at a fast central synapse. *Neuron* **20,** 797–807 (1998).
4. Abbott, L. F., Varela, J. A., Sen, K. & Nelson, S. B. Synaptic depression and cortical gain control. *Science* **175,** 220–224 (1997).
5. Tsodyks, M. V. & Markram, H. The neural code between neocortical pyramidal neurons depends on neurotransmitter release probability. *Proc. Natl Acad. Sci. USA* **94,** 719–723 (1997).
6. Lee, A. *et al.* Ca^{2+}/calmodulin binds to and modulates P/Q-type calcium channels. *Nature* **399,** 155–159 (1999).
7. Lee, A., Scheuer, T. & Catterall, W. A. Ca^{2+}/calmodulin-dependent facilitation and inactivation of P/Q-type Ca^{2+} channels. *J. Neurosci.* **20,** 6830–6838 (2000).
8. Peterson, B. Z., DeMaria, C. D., Adelman, J. P. & Yue, D. T. Calmodulin is the Ca^{2+} sensor for Ca^{2+}-dependent inactivation of L-type calcium channels. *Neuron* **22,** 549–558 (1999).
9. Chao, S. H., Suzuki, Y., Zysk, J. R. & Cheung, W. Y. Activation of calmodulin by various metal cations as a function of ionic radius. *Mol. Pharmacol.* **26,** 75–82 (1984).
10. Colecraft, H. M., Patil, P. G. & Yue, D. T. Differential occurrence of reluctant openings in G-protein-inhibited N- and P/Q-type calcium channels. *J. Gen. Physiol.* **115,** 175–192 (2000).
11. Zuhlke, R. D., Pitt, G. S., Deisseroth, K., Tsien, R. W. & Reuter, H. Calmodulin supports both inactivation and facilitation of L-type calcium channels. *Nature* **399,** 159–162 (1999).
12. Zuhlke, R. D., Pitt, G. S., Tsien, R. W. & Reuter, H. Ca^{2+}-sensitive inactivation and facilitation of L-type Ca^{2+} channels both depend on specific amino acid residues in a consensus calmodulin-binding motif in the α_{1C} subunit. *J. Biol. Chem.* **275,** 21121–21129 (2000).
13. Qin, N., Olcese, R., Bransby, M., Lin, T. & Birnbaumer, L. Ca^{2+}-induced inhibition of the cardiac Ca^{2+} channel depends on calmodulin. *Proc. Natl Acad. Sci. USA* **96,** 2435–2438 (1999).
14. Peterson, B. Z. *et al.* Critical determinants of Ca^{2+}-dependent inactivation within an EF-hand motif of L-type Ca^{2+} channels. *Biophys. J.* **78,** 1906–1920 (2000).
15. Houdusse, A. & Cohen, C. Target sequence recognition by the calmodulin superfamily: implications from light chain binding to the regulatory domain of scallop myosin. *Proc. Natl Acad. Sci. USA* **92,** 10644–10647 (1995).
16. Elshorst, B. *et al.* NMR solution structure of a complex of calmodulin with a binding peptide of the Ca^{2+} pump. *Biochemistry* **38,** 12320–12332 (1999).
17. Ehlers, M. D., Zhang, S., Bernhardt, J. P. & Huganir, R. L. Inactivation of NMDA receptors by direct interaction of calmodulin with the NR1 subunit. *Cell* **84,** 745–755 (1996).
18. Putkey, J. A., Sweeney, H. L. & Campbell, S. T. Site-directed mutation of the trigger calcium-binding sites in cardiac troponin C. *J. Biol. Chem.* **264,** 12370–12378 (1989).
19. Mori, M. *et al.* Novel interaction of the voltage-dependent sodium channel (VDSC) with calmodulin: does VDSC acquire calmodulin-mediated Ca^{2+}-sensitivity? *Biochemistry* **39,** 1316–1323 (2000).
20. Keen, J. E. *et al.* Domains responsible for constitutive and Ca^{2+}-dependent interactions between calmodulin and small conductance Ca^{2+}-activated potassium channels. *J. Neurosci.* **19,** 8830–8838 (1999).
21. Fanger, C. M. *et al.* Calmodulin mediates calcium-dependent activation of the intermediate conductance KCa channel, IKCal. *J. Biol. Chem.* **274,** 5746–5754 (1999).
22. Erickson, M. G. & Yue, D. T. FRET reveals tethering of calmodulin to calcium channel complex in single living cells. *Biophys. J.* **80,** 196a (2001).
23. Rodney, G. G. *et al.* Calcium binding to calmodulin leads to an N-terminal shift in its binding site on the ryanodine receptor. *J. Biol. Chem.* **276,** 2069–2074 (2001).
24. Barth, A., Martin, S. R. & Bayley, P. M. Specificity and symmetry in the interaction of calmodulin domains with the skeletal muscle myosin light chain kinase target sequence. *J. Biol. Chem.* **273,** 2174–2183 (1998).
25. Kink, J. A. *et al.* Mutations in paramecium calmodulin indicate functional differences between the C-terminal and N-terminal lobes in vivo. *Cell* **62,** 165–174 (1990).
26. Ohya, Y. & Botstein, D. Diverse essential functions revealed by complementing yeast calmodulin mutants. *Science* **263,** 963–966 (1994).
27. Sutton, K. G., McRory, J. E., Guthrie, H., Murphy, T. H. & Snutch, T. P. P/Q-type calcium channels mediate the activity dependent feedback of syntaxin-1A. *Nature* **401,** 800–804 (1999).
28. Kincaid, R. L., Billingsley, M. L. & Vaughan, M. Preparation of fluorescent, cross-linking, and biotinylated calmodulin derivatives and their use in studies of calmodulin-activated phosphodiesterase and protein phosphatase. *Methods Enzymol.* **159,** 605–626 (1988).
29. Patil, P. G., Brody, D. L. & Yue, D. T. Preferential closed-state inactivation of neuronal calcium channels. *Neuron* **20,** 1027–1038 (1998).
30. Song, L. S., Sham, J. S., Stern, M. D., Lakatta, E. G. & Chang, H. Direct measurement of SR release flux by tracking 'Ca^{2+} spikes' in rat cardiac myocytes. *J. Physiol. (Lond.)* **512,** 677–691 (1998).

Supplementary information is available on *Nature*'s World-Wide Web site (http://www.nature.com) or as paper copy from the London editorial office of *Nature*.

Acknowledgements

We thank W. Agnew, C. Chen, H. Colecraft, M. Erickson, S. Takahashi, H. Agler and E. Sobie for discussion; B. Peterson for initial attempts to detect P/Q-type channel facilitation; and T. Snutch for the gift of human α_{1A} clone. This work was supported by an NIH NRSA fellowship (C.D.D.) and grants from the NIH (D.T.Y.) and NNI (T.W.S.).

Correspondence and requests for materials should be addressed to D.T.Y. (e-mail: dyue@bme.jhu.edu).

B cells acquire antigen from target cells after synapse formation

Facundo D. Batista, Dagmar Iber & Michael S. Neuberger

Medical Research Laboratory of Molecular Biology, Hills Road, Cambridge, CB2 2QH, UK

Soluble antigen binds to the B-cell antigen receptor and is internalized for subsequent processing and the presentation of antigen-derived peptides to T cells[1]. Many antigens are not soluble, however, but are integral components of membrane; furthermore, soluble antigens will usually be encountered *in vivo* in a membrane-anchored form, tethered by Fc or complement receptors[2–4]. Here we show that B-cell interaction with antigens that are immobilized on the surface of a target cell leads to the formation of a synapse and the acquisition, even, of membrane-integral antigens from the target. B-cell antigen receptor accumulates at the synapse, segregated from the CD45 co-receptor which is excluded from the synapse, and there is a corresponding polarization of cytoplasmic effectors in the B cell. B-cell antigen receptor mediates the gathering of antigen into the synapse and its subsequent acquisition, thereby potentiating antigen processing and presentation to T cells with high efficacy. Synapse formation and antigen acquisition will probably enhance the activation of B cells at low antigen concentration, allow context-dependent antigen recognition and enhance the linking of B- and T-cell epitopes.

To investigate the B-cell response to antigen encountered as part of an immune complex tethered to a cell surface, immune complexes comprising hen-egg lysozyme (HEL) aggregated with specific immunoglobulin-γ (IgG) monoclonal antibodies were loaded on to the surface of an Fcγ receptor (FcγR)-expressing myeloid cell line. The immune complexes had a patchy distribution over the myeloid cell surface (Fig. 1a, b); however, on incubation with antigen-specific B cells, cell aggregates were formed in which the immune complexes on the myeloid cell and the B-cell antigen receptor (BCR) on the B cell were gathered together into a region of synapsis (Fig. 1c, d).

Similar results were obtained using immune complexes loaded onto FcγRI-expressing L-cell transfectants. Immunocytochemistry suggested that there is a gathering of tethered immune complexes, mediated by the BCR (possibly aided by the oligomeric nature of the BCR[5]) and accompanied by an apparent reorganization of the B-cell surface, as judged by segregation of the BCR from CD45 in the region of synapsis (Fig. 1e).

This concentration of BCR is reminiscent of the capping of surface IgM that results from incubation of B cells with polyvalent anti-IgM antisera[6,7]. We therefore determined whether the reorganization of the B cell depended on the polyvalent nature of the immune complex. We generated transfectants displaying HEL antigen as a presumptively monovalent integral membrane antigen and used one of these transfectants (J[mHEL]6; Fig. 2a) in excess as a target for HEL-specific B cells. Confocal microscopy showed that, after 10 min, most B cells were in conjunction with a target; BCR was concentrated in the region of synapsis but with clear exclusion of CD45 (Fig. 2b, c, f; Supplementary Information movie 1).

Reorganization of components of the B-cell membrane was also evident from a depletion of CD22 from the centre of most synapses (although often concentrated at the edges), where there was a concentration of ganglioside GM1 (which is associated classically with many Src-family tyrosine kinases). There was also polarization of cytoplasmic components, as judged by a depletion of the signal-inhibitory phosphatase SHP1 in the region of the synapse (Fig. 2d–f), but a concentration of phosphotyrosine-containing proteins as well